The Mechanics of a Cantilever Beam with an Embedded Horizontal Crack Subjected to an End Transverse Force, Part B: Results and Discussion

Panos G. Charalambides [1]   and Xiaomin Fang [1]

1 – Department of Mechanical Engineering, The University of Maryland, Baltimore County,1000 Hilltop Circle, Baltimore, MD 21250, USA

ABSTRACT. This is the second part of a two-part study aimed at establishing the mechanics of a cracked cantilever beam subjected to a transverse force applied at its free end. Following the development of a four-beam model in Part A, in this Part B of a two Part series of papers, a two dimensional (2D) Finite Element (FE) model is developed and use to obtain independent numerical estimates of the cross sectional resultants dominating the beams above and below the fully embedded horizontal crack in a cantilever beam subjected to an end transverse force. The FE model is also used to obtain numerical estimates of the required deformation of the cantilever free as needed to establish the effective of the transition regions adjacent to the crack tips. The FE model results are then compared to the four-beam model predictions. The four-beam model predictions are found to be in excellent agreement with their FE counterparts. Related discussion is presented wherein the relevance of the model developed in Part A to damage and crack detection as well as to fundamental fracture mechanics studies on homogeneous and heterogeneous layer systems containing delamination cracks is addressed.

Introduction. The background and motivation of this study are presented in Part A [1] of this two-part series of papers. As discussed in [1], the development of a simple but robust mechanics of materials model for the cracked system considered in this study is motivated by the need to develop robust damage and crack detection [2-19] diagnostic tools and capabilities that are needed in assessing the structural integrity of components and structures. While ample research has been undertaken in the above areas, simple to use and implement models and methods are still required for the timely detection of both diffused damage as well as the presence of cracks in such systems. In light of the above, this study is expected to contribute in the development of such tools that are based both on physics based models as well as on non-model based methods primarily based on damage and crack induced free surface curvature changes as discussed elsewhere [20-23]. The focus of this Part B of the two-part series of papers is to conduct parametric studies using the model develop in [1] while also developing independent 2D FE model predictions needed to calibrate the model developed in [1] and present comparisons between the four-beam model predictions and the 2D FE estimates.

In Part A [1] of this two-part series of papers, a four-beam model was developed capable of capturing the load transfer mechanics through the near-tip Transition regions for a cantilever beam containing a horizontal crack and subjected to an end loading force. As discussed above, the model

developed in [1] will be employed in this study in obtaining cross-sectional resultants dominating the beam area in the crack region while also using the model findings to better understand the load transfer mechanics through the same crack region for the system under consideration. In doing so, a summary of the key findings of the four-beam model developed in [1] shall be presented next.

Key findings of the four-beam model. The four-beam model reported in [1] was developed for the cracked cantilever beam shown in Fig. 1a. Overall, the beam has a length L, height h while containing a horizontal sharp crack of length $l = 2a$ located at position x_C from the fixed end at depth h_1 from the top surface. Consistent with the four-beam model developed in [1], the above domain was divided into four sub-domains, each forming a beam as shown in Fig. 1a labeled Beam-1, Beam-2, Beam-3 and Beam-4. Transition regions 1 through 4 were introduced, the effective deformation of which was assumed to be captured by rotary springs placed at Beam Interfaces 1 through 4 shown in Figs. 1 and 2. The model developed in [1] employed the following beam deformation findings established via the method of finite elements in [18]:

(a) The free surface and neutral axis curvatures of the cracked beam at the crack center location match the curvature of a healthy beam, i.e., an identical beam without a crack under an end force condition;

(b) The neutral axis rotations (slope) of the cracked beam in the region between the applied load and the nearest crack tip matches the corresponding slope of the healthy beam.
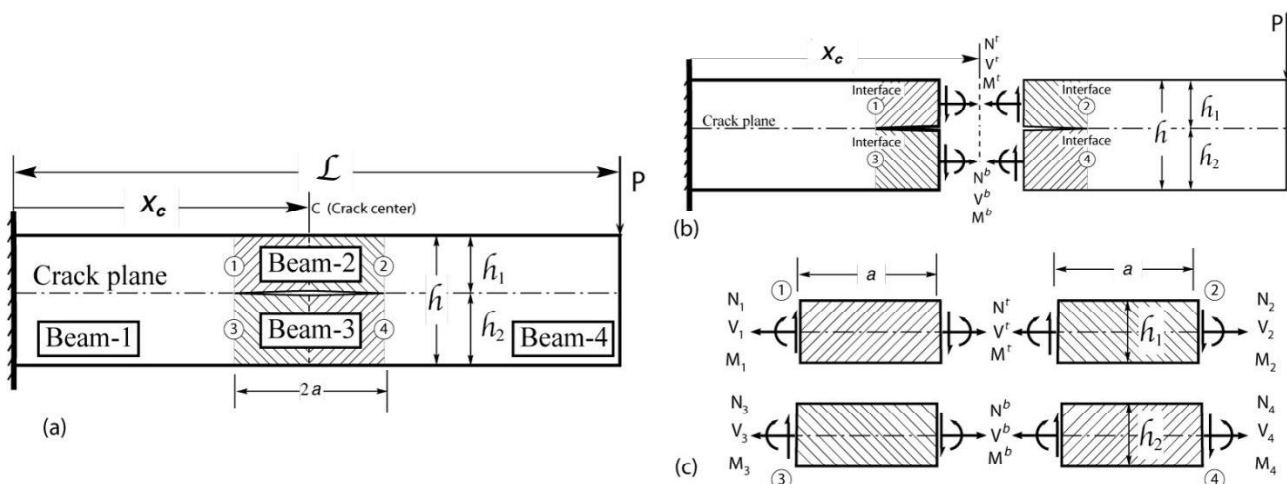

Fig. 1. Schematics used in the development of the analytical model capturing the mechanics of the beams above and below the crack, i.e., Beams 2 and 3 shown above. (a) The cracked beam with Beams 2 and 3 highlighted along with Interfaces 1-4. (b) A section through the center of the crack exposing the force and moment resultants acting in the "top" and "bottom" beams. (c) Free body diagrams of the left and right half of the "top" and "bottom" beams, exposing the resultants acting at their corresponding Interfaces 1-4.

Based on the finding (a) above, curvature matching of Beams 2 and 3, i.e., the beams above and below the horizontal crack also referred to as the top and bottom beams respectively, with that of the healthy beam yields the following beam resultant moment equations:

$$M^t = \frac{I_t}{I} M_C \text{ and } M^b = \frac{I_b}{I} M_C \tag{1}$$

where M^t is the moment resultant at the crack center cross section dominating the "top" beam or Beam-2;

M^b is its counterpart dominating the "bottom" beam or Beam-3 as shown in Fig. 1b;

M_C is the resultant bending moment transferred through the cross section at the crack center location in the healthy beam, i.e., an identically loaded and supported beam without a crack.
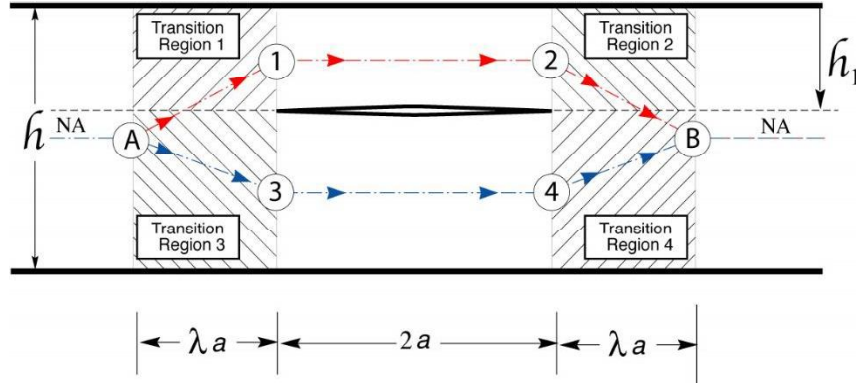

Fig. 2. The compatibility paths followed through the "top" and "bottom" beams in establishing angle of rotation and deflection compatibility conditions from reference section A to reference section B. Also shown are Transition Regions 1-4.

For a downward load P the bending moment at the crack center location in the healthy beam is $M_c = -P(L-x)$. The quantities I_t, I_b, and I are the second moments of inertia for the top, bottom, and healthy beams respectively. With the bending moments acting in the top and bottom beams known, an expression for the axial forces N^t and N^b is then obtained through a global moment equilibrium enforced over the right half of the beam as discussed in [1] (see Fig. 1), such that,

$$N^b = -N^t = \frac{2M_C}{h}\left\{1 - \frac{I_t + I_b}{I}\right\}$$

(2)

As shown in Fig. 1, at the crack center cross sections, Beam-2, i.e., the beam above the crack plane, is subjected to an axial force resultant N^t, shear force resultant V^t and bending moment resultant M^t. Similarly, Beam-3 also referred to in this study as the bottom beam denoted by a superscript $()^b$ or subscript $()_b$, is subjected to force and moment resultants N^b, V^b and M^b respectively. Meanwhile, Section/Interface 1 which is the left end of the top beam is subjected to the force and moment resultants N_1, V_1 and M_1 whereas the right end of the same beam is subjected to N_2, V_2 and M_2 at Interface 2. Similarly, the bottom beam or Beam-3 is subjected to end forces and moments N_3, V_3 and M_3 at Section/Interface 3 and N_4, V_4 and M_4 at Section 4 as shown in Fig. 1c.

As presented in [1], beam deflection and beam slope compatibility conditions along with the finding (b) above, (i.e., slope matching of the cracked and healthy beams at the end of the Transition region to the right of the right crack tip), yield the following shear force equation,

$$\frac{V_t}{V_b} = \frac{l_t}{l_b} \frac{\lambda(2+\lambda) + 2(1+\lambda) + \dfrac{2}{k_b} \dfrac{l_b}{A_b a^2} \dfrac{E}{G}}{\lambda(2+\lambda) + 2(1+\lambda) + \dfrac{2}{k_t} \dfrac{l_t}{A_t a^2} \dfrac{E}{G}} \qquad (3)$$

where λa is the length of the transition regions (see Fig. 2);

   $2a$ is the crack length.

Also in the above equation, I represents the second moment of inertia, A is the related cross sectional area, E is the modulus of elasticity, G is the shear modulus and k is the Timoshenko shear constant [17]. The subscripts $(\ )_t$ and $(\ )_b$ denote quantities for the beams above (top beam or Beam-2) and below (bottom beam or Beam-3) the crack. As discussed in [1], it is worth noting that when ignoring the Timoshenko shear effects, i.e., letting k_t and $k_b \to \infty$ then the following simple form for the shear force ratio which becomes independent of the transition region length proportionality constant λ, is obtained, i.e.,

$$\frac{V_t}{V_b} = \frac{I_t}{I_b} \qquad (4)$$

It is also noteworthy to observe for systems in which the crack is on the beam neutral axis (i.e., $h_1 = h_2$), both Eqns. (3) and (4) predict that the shear force ration between the shear resultants in the top and bottom beam is $V_t/V_b = 1$ and thus from global equilibrium it can be shown that $V_t = V_b = P/2$. As will be discussed later in this study, shear force predictions obtained by the present model were found to compare very well with 2D finite element results.

In [1], the transition region length proportionality constant λ, is obtained by matching the deflection at the free end of the cracked beam predicted by the four-beam model to its counterpart obtained independently using a 2D FE model. This consistency condition gives rise to a non-linear equation in λ which can then be solved for admissible values of λ. The above consistency equation is fully derived in [1] and is summarized below.
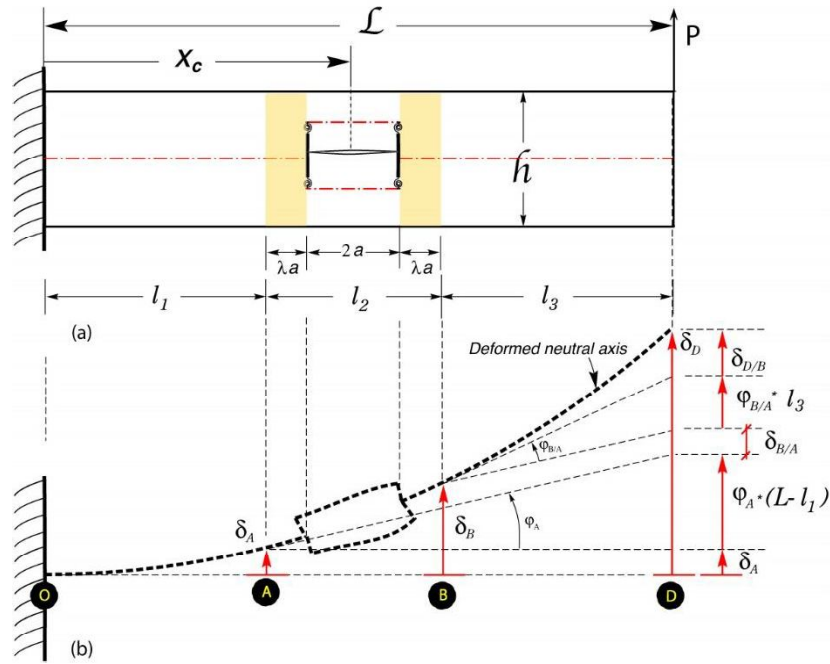
Fig. 3. A schematics showing (a) the original cracked beam with its un-deformed neutral axis and (b) the deformed neutral axis configuration of the four-beam model. The relationship between the deflections and rotations at key reference points of the beam are also shown in (b). The deformations and rotations between A and B include the transition region effects captured by the rotary spring and Timoshenko shear effects.

With the aid of the schematic shown in Fig. 3 and as presented in [1], the following consistency equation applies,

$$\delta_D^{MM} = -\frac{(1-\nu^2)PL^3}{EI}\left\{\frac{1}{3}\hat{l}_1^3 + \frac{1}{2}(1-\hat{l}_1)\hat{l}_1^2 + \frac{(\hat{l}_1+\hat{l}_3)(1+\nu)}{6k}\left(\frac{h}{L}\right)^2 + \left(\frac{1}{2}\hat{l}_1^2 + (1-\hat{l}_1)\hat{l}_1\right)(1-\hat{l}_1)\right.$$

$$+ (1-\hat{x}_C)\hat{a}^2(2+4\lambda+\lambda^2) + \frac{V_t}{P}\frac{I}{I_t}\hat{a}^3\left(\frac{2}{3}+\lambda(2+\lambda)\right) + \frac{V_t}{P}\frac{\hat{a}(1+\nu)}{3k_t}\left(\frac{h}{L}\right)^2\frac{h}{h_1} \qquad (5)$$

$$\left. + \frac{\lambda\hat{a}(1+\nu)}{6k}\left(\frac{h}{L}\right)^2 + (1-\hat{x}_C)2\hat{a}(1+\lambda)\hat{l}_3 + \frac{1}{3}\hat{l}_3^3 = -\frac{PL^3}{EI}\left\{\frac{1}{12}\left(\frac{h}{L}\right)^3\delta^{FE}{}_D\right\}\right.$$

where δ_D^M is the beam deflection at its free end at D as shown in Fig. 3;

δ_D^{FE} is its 2D FE counterpart.

In the above equation, the ˆ symbol denotes non-dimensional values with all length quantities normalized with respect to the beam length L and $E' = E/(1-\nu^2)$ is used to convert the beam plane stress to its plane strain equivalent solution. Also in the above consistency equation, $\hat{\delta}_D{}^{FE}$ is the absolute value of the deflection of the cracked beam at its free end obtained through non-

dimensional FE simulations as will be discussed later in the study. Also in Eqn. (5), $I_1 = L - (x_c - a(1+\lambda))$, $l_2 = 2a(1+\lambda)$ and $I_3 = L - (x_c + a(1+\lambda))$, $M_t / I_t = M_c / I$ and $M_c = -P(L - x_c)$. Furthermore, V_t can be expressed in terms of the load P and the shear force ratio V_t / V_b given by Eqn. (3). In Eqn. (5), the constants k and k_t are the Timoshenko shear constants for the healthy beam and Beam-2 above the crack respectively. Thus using the above equations and after normalizing each term with respect to a characteristic deflection $\Delta = PL^3 / E'I$, the following consistency condition in which the only unknown is the transition region length constant $\square$ is obtained,

$$\alpha(\lambda)\lambda^2 + \beta(\lambda)\lambda + \eta(\lambda) = 0 \tag{6}$$

where the equation coefficients are functions of $\square$ either explicitly as shown below or implicitly through the beam lengths $\hat{l}_1(\lambda), \hat{l}_2(\lambda), \hat{l}_2(\lambda)$ and are given by,

$$\alpha(\lambda) = (1 - \hat{x}_C)\hat{a}^2 + \frac{\gamma I}{I_b + \gamma I_t}\hat{a}^3$$

$$\beta(\lambda) = 4(1 - \hat{x}_C)\hat{a}^2 + 2\frac{\gamma I}{I_b + \gamma I_t}\hat{a}^3 + 2(1 - \hat{x}_C)\hat{a}\hat{l}_3 + \frac{\hat{a}(1+\nu)}{6k}\left(\frac{h}{L}\right)^2$$

$$\eta(\lambda) = \frac{1}{3}(\hat{l}_1^3 + \hat{l}_3^3) + (1 - \hat{l}_1)\hat{l}_1^2 + \hat{l}_1(1 - \hat{l}_1)^2 + 2\hat{a}(1 - \hat{x}_C)(\hat{a} + \hat{l}_3)$$

$$+ \frac{V_t}{P}\left[\frac{2}{3}\frac{I}{I_t}\hat{a}^3 + \frac{(1+\nu)\hat{a}}{3k_t}\left(\frac{h}{L}\right)^2\frac{h}{h_1}\right] + \frac{(1+\nu)(\hat{l}_1 + \hat{l}_3)}{6k}\left(\frac{h}{L}\right)^2 \tag{7}$$

$$- \frac{1}{12(1-\nu^2)}\left(\frac{h}{L}\right)^3 \delta_D^{FE}$$

where $\gamma(\lambda)$ is a subset of Eqn. (3) and is given by,

$$\square(\square) = \frac{\square(2 + \square) + 2(1 + \square) + \dfrac{2}{k_b}\dfrac{I_b}{A_b a^2}\dfrac{E}{G}}{\square(2 + \square) + 2(1 + \square) + \dfrac{2}{k_t}\dfrac{I_t}{A_t a^2}\dfrac{E}{G}} \tag{8}$$

In the above equation, the finite element term is divided by the $(1-v^2)$ factor as needed to match the beam plane stress and the 2D FE plane strain solutions. The above consistency equation in λ will be solved for several cases wherein the horizontal crack is placed at different locations along the length and height of the beam. However, in order to carry out this task, finite element solutions for the non-dimensional deflection of the beam at the free end will need to be obtained. Thus, a brief description of the finite element models used in these simulations shall be discussed next.

Finite Element modeling of a beam with a horizontal crack. Broad finite element studies of a cantilever beam containing a fully embedded sharp crack and subjected to end transverse loading and bending moment have been carried out as reported in [18,19]. In those studies, cracks of varying length and orientation were systematically placed at various geometrically admissible locations within the beam. The near tip mechanics both at the left and right crack tips were established while neutral axis, as well as top and bottom surface deflections, slopes and curvatures were also established. The finite element results reported in this study compliment those reported in [18] and [19] in that they help in the development of a better understanding of the load transfer mechanism across the crack region in the areas above and below the crack as well as within the transition regions near the crack tip regions. For completeness, specifics of the finite element modeling used in deriving the results reported in this study shall be presented next.

As shown in Fig. 4, a 2D rectangular domain of length L and height h with a horizontal sharp crack of length $l = 2a$ with its center located at position x_C from the left fixed end and at depth h_1 from the top surface was discretized using 4-noded isoparametric elements under plane strain conditions. A generalized mesh generator developed in [18] was used. Care was given to the meshing of the near-tip regions using a converging "spider web" with a minimum of 16 rings of elements all placed within a small region as needed to capture sufficient details of the near-tip singular fields. A vertical transverse load P was applied at the top left corner of the mesh as shown in Fig. 4. The finite element simulations were carried out in a non-dimensional environment as discussed in [18,19], where the length of the beam L was taken to be the characteristic length, its elastic modulus was taken to be the characteristic modulus with a Poisson's ration $v = 0.3$ and the intensity of the applied load P was taken to be the characteristic line force. Fig. 4 shows five FE models in which a crack of length $2a = 0.2L$ is shown to be placed at $x_C = 0.4L$ and at various depths as measured by the parameter h_1/h. For example, the top FE model corresponds to $h_1/h = 0.7$ whereas the bottom mesh represents a beam containing a shallow crack relative to the top surface with $h_1/h = 0.3$. All FE simulations reported in this study were carried out for a beam with an $h/L = 0.1$ aspect ratio.

As a means of comparing the four-beam model predictions to the 2D finite element results, the normalized axial force resultants N^t/P and N^b/P along with the shear counterparts V^t/P and V^b/P as well as the equivalent bending moment acting at the mid-plane of the regions above and below the crack surface, M^t/PL and M^b/PL respectively were calculated using finite element stress estimates. In doing so, finite element stresses were extracted at the Gauss integration stations nearest to the vertical plane passing through the crack center using elements from both sites of the above vertical plane. Finite element stress estimates from adjacent stations were then averaged and were then numerically integrated along the height of the individual beam (Beams 2 and 3 above the below the crack plane respectively as shown in Fig. 2) as needed to obtain the stress resultants reported herein.

In addition to obtaining finite element estimates of the force and moment resultants, the deflection at the free end of the cracked beam for each model was also extracted. Those results were reported in [18]. As discussed above, an independent finite element estimate of the beam deflection is needed in calibrating the four-beam model developed in this study. Furthermore, deflection, slope and curvature results along the top free surface of a cracked beam reported in [18] provide evidence of the two critical observations employed in the model development. The above finite element results along with the model predictions shall be presented next.

Results. Cross sectional force and moment resultants as well as effective transition region length predictions obtained using the four-beam model are reported in Figs. 5 through 8 where their finite element counterparts are also reported.

For example, Fig. 5 shows the normalized moment resultants M^t/PL and M^b/PL as a function of the normalized crack depth h_1/h in the 0.25 to 0.75 range. The analytical predictions obtained through Eqn. (3) are shown using solid lines whereas the finite element results are shown using discrete symbols. Three sets of data obtained for $x_C/L = 0.3, 0.4$ and 0.5 are reported. It may be of importance to recall that the model developed in [1] and summarized in this study is based on the fundamental observation of matching curvatures at the cross sections located at the crack center. That observation led to the development of the moment equation given by Eqn. (1) which was used to obtain the analytical moment predictions reported in Fig. 5. As shown, the analytically predicted moment resultants are in excellent agreement with those obtained using finite elements. This finding validates the fundamental assumption made in the model development and further reinforces the notion that simple but robust models can be developed in understanding the seemingly complex behavior of cracked structures. As expected, the beams above and below the crack are shown to experience equal amounts of bending moments predicted to be $1/8$ of the bending moment experienced by the healthy beam at the crack center location when $h_1/h = 0.5$. while a higher portion of the moment is predicted to be transferred through the thicker of the two beams when $h_1 \neq h_2$.
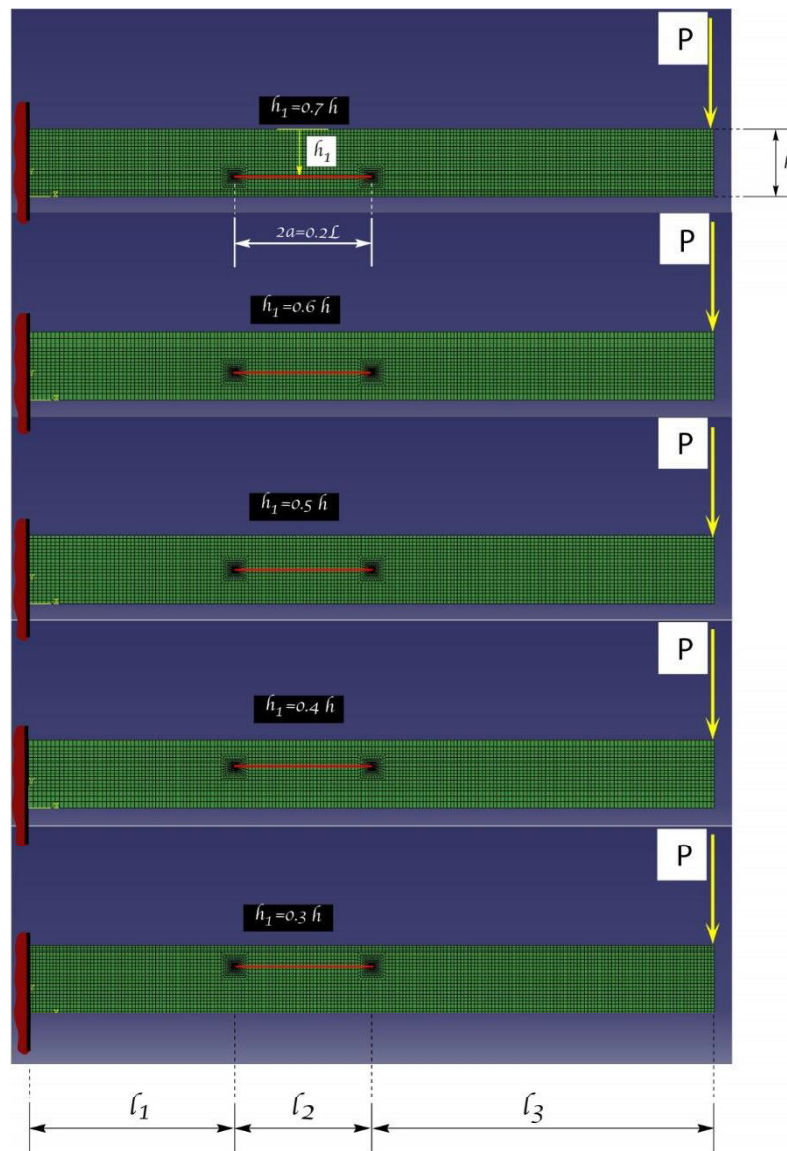
Fig. 4. Two dimensional finite element models used in extracting force and moment resultants as well as the free-end deflections used in model calibration and comparison studies reported in Figs. 5-10 below. As shown, the fixed conditions were imposed on the left edge of the beam whereas a downward transverse load P was applied at the top right corner of each mesh. The various models shown represent beams containing horizontal cracks of length $2a = 0.2L$ at various depths, with a beam aspect ratio h/L=0.1 as reported in [18].
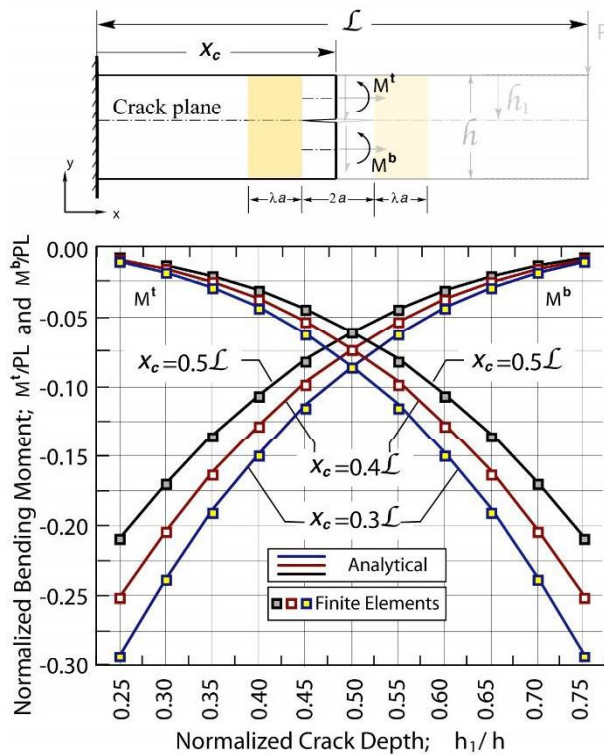
Fig. 5. Normalized bending moment resultants plotted against the crack depth ratio h_1/h predicted for the "top" and "bottom" beams in the crack region. The discrete points were obtained via 2D finite element simulations using model similar to those presented in Fig. 4. The solid lines were obtained using Eqn. (1). The results correspond to a downward load P. Results for three different crack center locations, i.e., $x_C/L = 0.3, 0.4$ and 0.5 are presented. The curves with the upward trend correspond to the moment M^b in the bottom beam, whereas the results with the downward trend correspond to the moment M^t in the top beam.
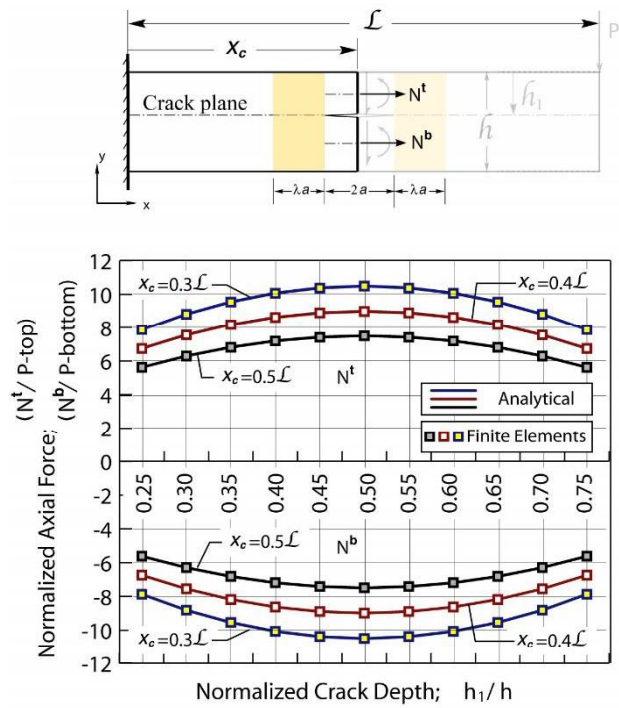
Fig. 6. Normalized axial force resultants plotted against the crack depth ratio h_1/h predicted for the "top" and "bottom" beams in the crack region. The discrete points represent 2D finite element predictions whereas the solid lines were obtained using Eqn. (2). The results correspond to a downward load P. The "top" beam is predicted to be in tension while the "bottom" beam is predicted to be in compression with a force of equal magnitude as that of the top beam. The curves with negative values correspond to the axial force N^b in the bottom beam, whereas the results with the positive values correspond to the axial force N^t in the top beam.

Fig. 6 shows the normalized axial force resultants N^t/P and N^b/P as a function of the normalized crack depth h_1/h again in the 0.25 to 0.75 range. The analytical predictions obtained through Eqn. (5) are shown using solid lines whereas the finite element results are shown using discrete symbols. As before, three sets of data obtained for $x_C/L = 0.3, 0.4$ and 0.5 are reported. The top set of curves correspond to the axial force N^t/P acting at the mid-plane of Beam-2 above the crack plane. The bottom set of curves correspond to the normalized resultant N^b/P acting at the mid-plane of Beam-3 below the crack plane. A remarkable agreement is shown to exist between the axial force predicted through Eqn. (2) and the finite element results for all instances considered. As expected, for a downward load P, Beam-2 above the crack plane is subjected to a tensile force whose magnitude scales with the distance of the crack center from the applied load P while inversely proportional to the beam height h consistent with Eqn. (5). Again, as expected, an equal

and opposite axial force is applied at the mid-plane of Beam-3 below the crack plane thus forming a couple with its counterpart acting in Beam-2 above the crack plane. When considering the results reported in Figs. 5 and 6, one recognizes that in the crack region the bending moment transfer through the cracked beam region takes place primarily through a couple with a pair of tensile and compressive forces acting at the mid-plane of the beams above and below the crack plane. It may also be important to note that once the resultant forces and moment N^t and M^t are known, their counterparts in the lower beam are established, through Eqns. (1) and (2).

The shear force resultants predicted both using the model developed in this study and through the method of finite elements are presented in Fig. 7. It is important to note that in order to establish the shear forces V^t and V^b acting in Beams 2 and 3 respectively, one needs to solve for the transition region length parameter $\square$ first using the consistency condition given by Eqn. (5). Once λ is established, then the shear force ratio can be obtained through Eqn. (3) and then use global force equilibrium as needed to obtain the individual shear forces V^t and V^b. So, for each case considered, the corresponding value for the deflection at the free end of the cracked beam was used to solve a non-linear equation in λ given by Eqn. (6). For the systems considered, the $\square$ values obtained with the aid of Eqn. (6) are reported in Fig. 8. However, the $\square$ trends will be discussed later on in this section while now focusing on the shear resultants shown in Fig. 7.

The shear force profiles plotted against the crack depth ratio h_1/h and predicted using the analytical model are shown in solid blue lines in Fig. 7. The finite element results are shown using the discrete symbols as marked on the same figure. As shown, the model predictions and finite element results exhibit the same overall trends. The results appear to be in excellent agreement for cracks located at or close to the mid-plane of the healthy beam. However, the analytical predictions appear to be slightly larger when compared to the finite element predictions for the shear force in the thicker beam while slightly underestimating its FE counterpart in the thinner of the two beams when $h_1 \neq h_2$. Maximum deviation of less than 8% in the thicker beams appears for systems in which $0.3 \leq h_1/h \leq 0.4$ or $0.6 \leq h_1/h \leq 0.7$. It may be of importance to note that the $\square$ and related shear force resultant results reported in this study were obtained using a Timoshenko constant $k_t = k_b = k = 0.856$ for the top, bottom and healthy beam respectively consistent with reported values for beams with a rectangular cross section [24, 25].

The λ curves obtained by solving Eqn. (6) and reported in [18] are plotted in Fig. 8. Some interesting observations can be made. For example, the normalized transition region length parameter λ is predicted to increase with the normalized crack depth h_1/h, acquiring a maximum at $h_1/h = 0.5$. A symmetric profile is predicted for cracks located at equal distance above or below the mid-plane of the healthy beam. The results also suggest that the transition region length does depend on the location of the crack center along the axis of the beam. Perhaps somewhat counter-intuitive is the model prediction that a shorter transition region is predicted for cracks located close to the fixed end of the beam as shown by the $x_C/L = 0.5, 0.4$ and 0.3 curves. It may also be important to note that for the case of $h_1/h = 0.5$, although for a slightly higher beam aspect ratio, i.e., $h/L = 0.2$, available finite element results reported in [18] suggest that the transition region length is approximately equal to $\lambda^{FE} a \approx 1.67a$ which suggest a value for $\lambda = 1.67$. As reported in [18] and shown in Fig. 8, the model prediction for the case of $x_C/L = 0.5$ and $h/L = 0.1$ is $\lambda = 1.615$ which is remarkably close to the value obtained through finite elements. The above results and general findings of this study are critically analyzed and discussed in the next section.

In order to further understand the transition region mechanics, profiles of the normalized bending moment transferred through the top portion of the beam along with the % difference between the moment carried by the crack beam and its "healthy" counterpart are plotted in Fig. 9.
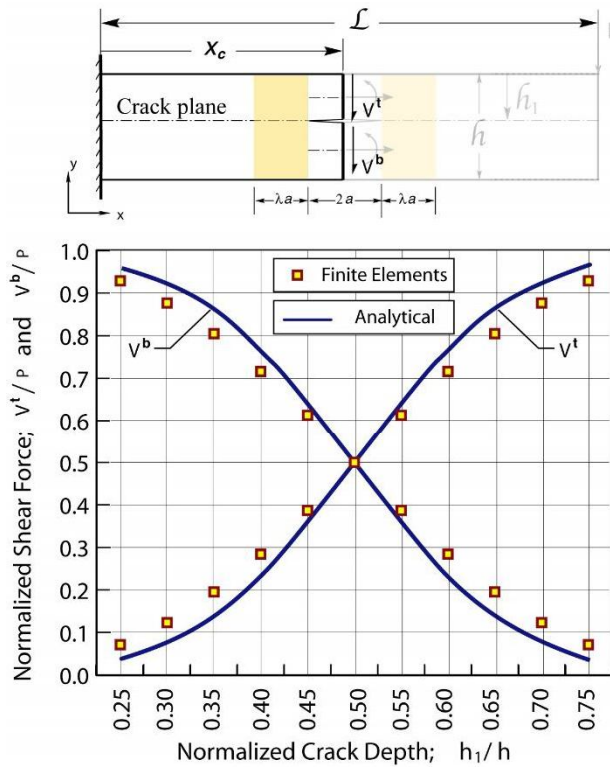

Fig. 7. Normalized shear force resultants plotted against the crack depth ratio h_1/h predicted for the "top" and "bottom" beams in the crack region. The discrete points represent 2D finite element results whereas the solid lines were obtained via Eqn. (3) and global force equilibrium. Both the finite element and analytical model simulations reproduced the same profiles for all crack center locations considered indicating that the shear forces depend only on the normalized crack depth h_1/h.
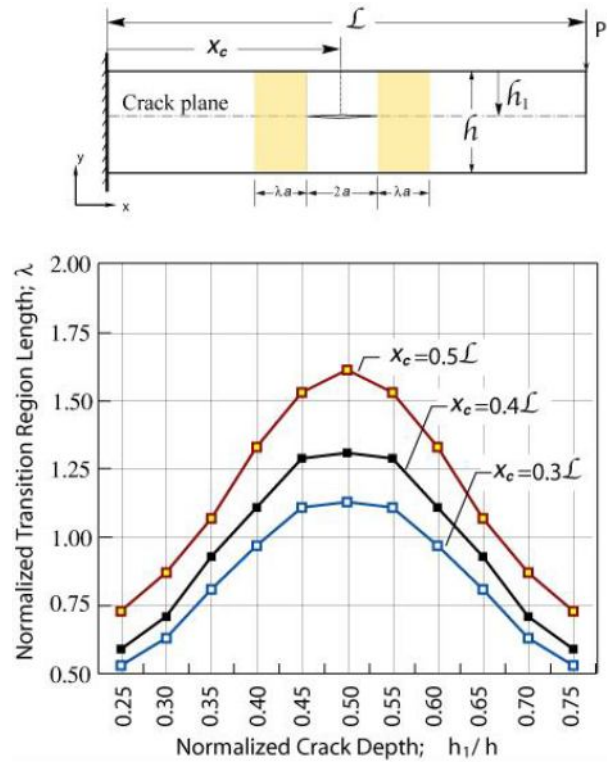
Fig. 8. The non-dimensional transition region length parameter λ plotted against the normalized crack depth h_1/h. Results obtained through the four-beam model for three different crack locations, i.e., $x_c/L=0.3$, 0.4 and 0.5 are presented. The discrete symbols represent the cases for which finite element deflections at the free end of the beam were used to solve for the crack length parameter λ
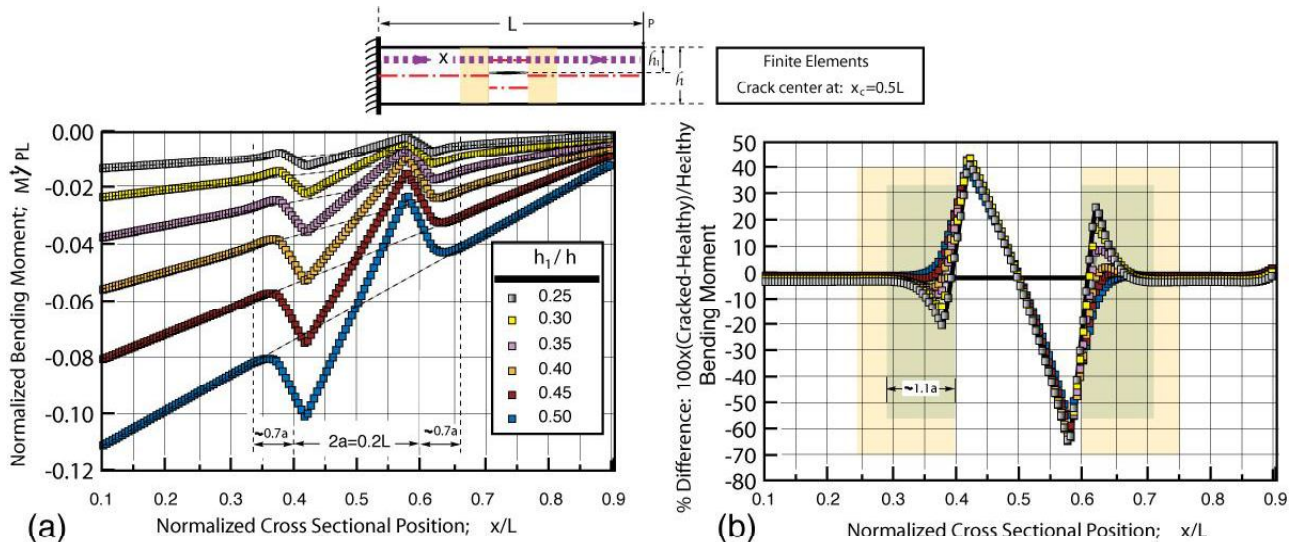
Fig. 9. (a) Profiles of the normalized bending moment carried by the "top" portion of the beam extracted from the FE models discussed in this study. Different curves correspond to beams with cracks placed at different h_1/h depths as indicated in the figure. (b) Profiles of the % difference of the bending moment carried by the top portion of the cracked beam to its "healthy" counterpart.

The results reported in Fig. 9a were extracted from the 2D FE models discussed earlier in this work. In obtaining these results, the normal stresses to cross sections along the path x indicated in the figure were first extracted from the FE model. Their contribution to the bending moment with respect to the neutral axis of the top beam was then integrated to obtain the moment resultant carried by the top beam, i.e., the beam above the embedded horizontal crack. A % difference between the moment carried by the cracked beam and its "healthy" counterpart was also calculated for each of the models considered in this study. The latter results are reported in Fig. 9b. In Fig. 9a, the straight dash lines represent the bending moment carried by the "healthy" beam. It is of interest to observe that the presence of the crack appears to cause a local change in the bending moment, and thus the beam curvature in the vicinity of the crack. The predicted moment change appears to extend at the most extreme case to approximately $0.7a$ to $1.1a$ (see Fig. 9a and 9b respectively) on either side of the crack. Similar results related to the axial and shear force profiles (see Fig. 10) suggest that the changes in the associate axial and shear force resultants may persist over somewhat greater extent to approximately $1.5a$ to $1.7a$ as shown in Fig. 10. The latter results would indeed be consistent with model transition region estimates reported herein. As shown, in Fig. 10, finite element profiles of the normalized axial force N^t/P and shear force V^t/P, transmitted through the top portion (i.e., beam above the crack plane) of the cracked beam are reported. Like in Fig. 9, the force resultants reported in Fig. 10 were extracted from FE models by integrating the normal and shear stresses acting on cross sections along the designated path x. The different curves correspond to beam systems containing a horizontal crack at different depths h_1/h as indicated in the figure. It may be of interest to observe that when comparing the profiles reported in Figs. 9 and 10, the shear force resultant appears to exhibit larger transition profiles when compared to either the bending moment or the axial force profiles.
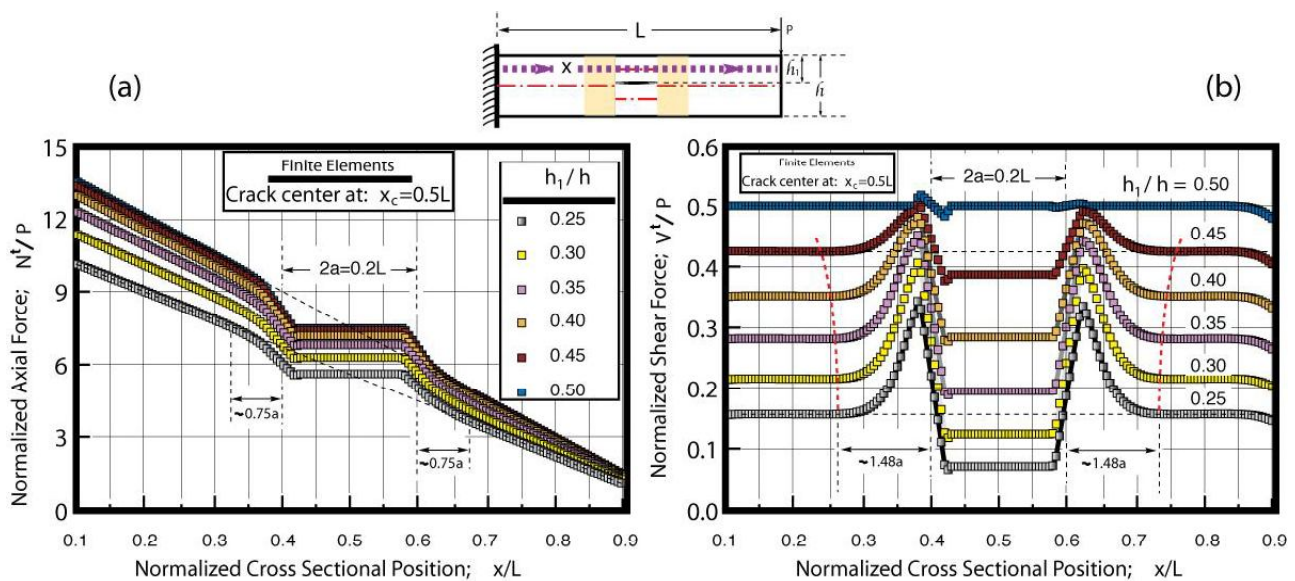

Fig. 10. Finite element profiles of the normalized axial force (a) and shear force (b), transmitted through the top portion (i.e., beam above the crack plane) of the cracked beam. The different curves correspond to beam systems containing a horizontal crack at different depths h_1/h as indicated in the figure.

The results reported in Fig. 9, may also have profound implications on the development of non-model crack detection methods [20-23], since, the predicted crack induced changes in the bending moment would cause reciprocal and measurable changes in the beam's surface curvatures.

Discussion. The four-beam mechanics of materials model developed in [1] is founded on two fundamental observations made possible through the method of finite elements, i.e., *(a) the matching of the curvatures of the beams above and below the crack to the curvature of the healthy beam at the crack center location,* and *(b) the matching of the beam slope of the crack beam to that of the healthy beam at the end of the transition region closest to the applied loading.* While the matching of the beam slopes has been discussed as part of the transition region load transfer and deformation mechanism in an earlier section of this study, no such consideration has thus far been given to the first fundamental observation of matching curvatures. In an effort to do so, let's consider the mechanics of the beams above and below the crack plane, i.e., Beams 2 and 3 respectively.

As suggested both by the model and finite elements, the cross sectional force and moment resultants acting at the mid-plane of Beams 2 and 3 at the crack center cross section are fixed and depend on the bending moment $M_C = -P(L-x_C)$ acting at the crack center location in the healthy beam as well as on the beam height h and crack depth h_1/h. As discussed above, the shear forces also may depend on the mechanics of the transition region. Regardless, once those quantities are established, it is of importance to recognize that both the shear and axial force resultants acting in Beams 2 and 3 remain constant throughout the crack region. On the other hand, the bending moment would vary linearly consistent as discussed in [1]. Given the fact that no net axial force is present in the healthy beam while the shear force is also constant under the loading considered in this study, moment equilibrium at the crack tip cross section would suggest that the moment M_1 acting at Interface 1 would not be equal to its healthy beam counterpart and thus would exhibit a discontinuity through a finite jump. At the same time, similar arguments made for the cross section at the right crack tip, i.e., Interface 2 would lead to the conclusion that a similar moment discontinuity between M_2 and its healthy beam counterpart of an equal and opposite amount exist at the right crack tip at Interface 2. In light of the linear moment profile within Beams 2 and 3, the moments dominating the latter beams will have to intersect with their healthy beam counterparts at the crack center location. Since these moments are given in terms of the moment of inertia ratio as expressed in Eqn. (1), it can be concluded that at least for homogeneous systems the moment matching is equivalent to the matching of curvatures of Beams 2 and 3 in the cracked region, to the curvature of the healthy beam at the crack center location. With the above in mind, one could make similar arguments in understanding the mechanics of cracked beams under other type of loadings or even heterogeneous biomaterial or multilayered beams including composite laminates.

Another issue of relevance for discussion is the introduction of a transition region in the model development along with the predicted trends in the normalized transition region length parameter $\lfloor/\rfloor$. The transition regions were introduced in this beam model development as a means of accounting for the complex load transfer and deformation mechanics in the vicinity of the singular fields in the crack tip region. As discussed earlier, evidence from finite element studies do support the existence of such transition regions [18]. It is encouraging to see that the model predictions, at least in the $h_1/h_2 = 1$ case, are very close to results obtained using 2D finite elements. Additional finite element results may in fact be needed in establishing higher confidence in the λ model predictions over a wide range of h_1/h_2 rations and crack center locations x_C/L. However, such broad comparisons are

beyond the scope of this study and are expected to be reported in future works. For relatively long cracks, i.e., $a > \min(h_1, h_2)$ one could explain the transition region dependency on the crack depth (see Fig. 8) as being driven by the characteristic length ratio h_1/h. However, it is not quite obvious, at least to the authors, why smaller transition region lengths are predicted for cracks located closer to the fixed end. One possible explanation is the fact that such cracks are subjected to higher bending moments at the crack center location which results in higher axial force and bending moments acting at the crack tip edge of the transition region. In this model development, the mechanics of the transition region are captured through rotary spring and Timoshenko shear equations consistent with Eqn. (13). The important aspect of this modeling approach is that the rotations resulting from the deformation mechanics in the transition region are taken to be proportional to the respective moments M_1, M_2, M_3 and M_4 which increase with decreasing x_C/L. Thus, for a fixed h_1/h_2 and otherwise similar cracked beam geometries, the current model would yield larger rotational angles in the transition region for cracks located closer to the fixed end. Thus, as result of rigid body motions, smaller transition region lengths may be required to match the free end deflections. This finding is possibly an artifact of the model used. An improved model may in fact be needed wherein the transition region rotations are set to be related to the moment change in the crack region rather than the total moments acting at each of the four transition region interfaces.

Although the $\square$ predictions may need to be better understood through further studies, the same model has provided useful insights regarding both the global mechanics of the cracked beam as well as the local transition region and crack region mechanics. It is of interest to know that a predictive model now exists in calculating the force and moment resultants N_i, V_i and M_i, $i = 1, ..., 4$ acting at Interfaces 1-4. With the above resultants and those acting on the opposite vertical edge of the transition region known, one can proceed to develop a better understanding of the transition fields and their local and global mechanical effects. For example, when focusing on the bottom edge of the transition region, one could start developing useful qualitative arguments regarding the profiles of the normal and shear stress and how they can be related to the singular crack tip fields. A simple schematic showing such potential profiles is presented in Fig. 11. As shown, and due to the fact that the axial force acting on the left edge of the referenced transition region is not equal to that acting on the right edge, i.e., $N_A^t \neq N_1$, force equilibrium in the x-direction would suggest that a shear stress must exist on the bottom edge of the transition region which is the crack plane ahead of the left crack tip. The shear stress induced by the transverse shear force P on the horizontal plane ahead of the left crack tip is known to equilibrate the axial force difference acting at the left and right edges of the transition region in the healthy beam. Since N_1 is not equal to its counterpart acting in the healthy beam, an additional shear stress must exist on the crack plane ahead of the left crack tip as needed for global equilibrium. Since no change in the transverse force acting in the beam takes place, this added shear must be induced by the mode II [26,27] singular stress field dominating the crack tip region since mode I induces no shear on the crack plane. This observation provides useful insights in how one can integrate the macro-mechanics of the crack region to the singular fracture fields induced in the crack-tip regions. For example, force equilibrium in the x-direction would take the form,

$$\Delta N_{A-1}^{healthy} - \Delta N_{A-1}^{cracked} = w \int_0^{\lambda a} \Delta \tau_{xy}(x) dx \tag{9}$$

where $\Delta N_{A-1}^{healthy}$ is the change of the axial force between Sections A and 1 in the healthy beam (see Fig. 2);

$\Delta N_{A-1}^{cracked}$ is its counterpart in the cracked beam;

w is the beam width;

$\Delta \tau_{xy}$ is the change in the shear stress on the crack plane ahead of the crack tip required for equilibrium.

Qualitative arguments can lead to the development of viable stress profiles. For example, as shown in Fig. 11, the profile of $\Delta \tau_{xy}$ in the transition region ahead of the crack tip should conform to the mode II driven shear stress close to the crack tip. At a critical distance from the crack tip, the stress profile must go through a stress transition region as needed to bridge the stress profile away from the crack tip to that close to the crack tip. While plausible transition stress profiles can be postulated for all stress components, the importance of this argument is to note that a relationship between the transition length $\square$ and the mode I and mode II stress intensity factors may exist and could be established through the structure of the transition fields.

As discussed earlier in this study, another relevant observation is that the presence of even a slight mode I component would induce a tensile normal stress if $K_I > 0$ associated with crack tip opening, or compressive if $K_I < 0$ associated with crack surface contact as shown schematically in Fig. 11. The presence of such a stress close to the crack tip will need to be offset by an opposite stress resultant away from the crack tip in the transition region. Such a stress profile would then induce a net moment ΔM on the plane ahead of the crack tip in the transition region which ought to be counter-balanced by an equal and opposite moment on the vertical left edge of the transition region. Such a moment change could explain the free surface curvature "bump" at the end of each transition region as predicted via finite elements and reported in [18]. Thus, the presence of such a curvature "bump" could indicate the existence of crack damage in the vicinity of such a measurement used in non-model damage detection methods [20-23].
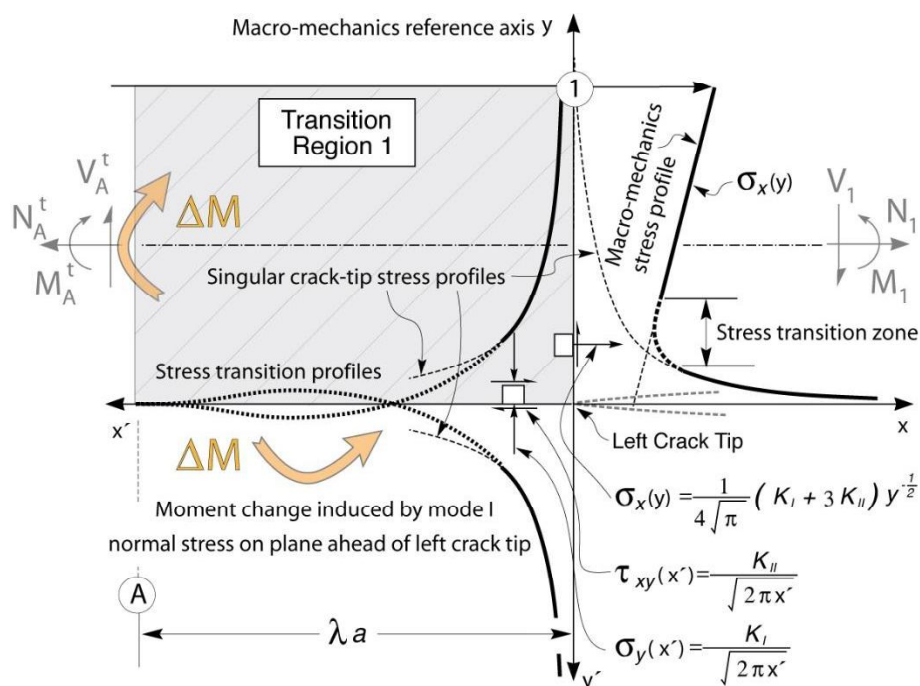
Fig. 11. Schematics of potential transition region stress fields that are superimposed onto those of the healthy beam. These fields are shown to conform to the near-tip mixed mode fields near the crack tip region and to the macro-mechanical field differences sufficiently away from the crack tip. As shown, a change of moment ΔM is induced by the mode I component of the stress intensity factor on the crack plane ahead of the left crack tip. An equal and opposite moment change then must occur on the left vertical plane of the transition region thus causing a slight "bump" on the moment and associated curvature profile at the start of the transition region as discussed in [1].

Finally in this section, it may also be important to note that this work is expected to have broader impact in advancing damage detection studies as well as studies on the fracture mechanics of structures with fully embedded cracks. For example, the macro-mechanics of the cracked beam established via the current model yield valuable information regarding the predicted free surface curvatures along the length of the beam. Enabled by the findings of this work, curvature deviations from an otherwise smooth profile measured experimentally, could be used to diagnose the presence of crack damage in structures as discussed elsewhere. Meanwhile, the near-tip mechanics can now be more thoroughly explored using analytical techniques such as the compliance method or the J-integral approach [26] in establishing the near-tip energy release rates and associated mode I and mode II stress intensity factors. Such studies have the potential to substantially enhance our understanding of mixed mode [28-30] and predominately mode II fractures while guiding improved designs of composites and composite laminate systems [29].

Summary. Informed by 2D finite element findings, a four-beam mechanics of materials model was developed in Part A [1] of this two-part series of papers. In this work, key findings of the four-beam model were first summarized. The development of related 2D FE models was then discussed and used to conduct parametric studies through which the cross sectional resultants acting in the beams above and below the crack were obtained. In addition, FE estimates of the cracked beam deflection at its free end were used to obtain the effective transition region length introduced in the development of the four beam model. Force and moment predictions were also obtained using the four-beam model which were then compared to their FE counterparts. The model and FE results were shown to be in excellent agreement over a wide range of crack location, i.e., depth from the top beam surface, and crack center location along the longitudinal axis of the beam.

The reported results show that the four-beam model is capable of predicting the load transfer and deformation mechanics of a cantilever beam containing a fully embedded horizontal crack under the application of an end transverse force. Discussion on the limitations of the model as well as its potential impact on damage detection and fracture of structures with embedded cracks is also included in this work.

References

[1] Charalambides, P.G. & Fang, X., The Mechanics of a Cantilever Beam with an Embedded Horizontal Crack Subjected to an end Transverse Force, Part A: Modeling, Mechanics, Materials Science & Engineering Journal ISSN 2412-5954, Vol.5, 2016, doi: 10.13140/RG.2.1.3874.4560

[2] Rizos, P.F., Aspragathos, N. & Dimarogonas, A.D. (1990). Identification of Crack Locations and Magnitude in a Cantilever Beam from Vibration Modes. *J. of Sound and Vibration*, *138(3)*, 381-388.

[3] Wong, C.N., Zhu, W.D. & Xu, G.Y. (2004). On an Iterative General-Order Perturbation Method for Multiple Structural Damage Detection. *Journal of Sound and Vibration*, *273*, 363-386, doi: 10.1016/S0022-460X(03)00543-1

[4] Xu, G.Y., Zhu, W.D. & Emory, B.H. (2007). Experimental and Numerical Investigation of Structural Damage Detection Using Changes in Natural Frequencies. *J. Vibration and Acoustics*, *129(6)*, 686-700, doi:10.1115/1.2731409

[5] He, K. & Zhu, W.D. (2011). A Vibration-based Structural Damage Detection Method and Its Applications to Engineering Structures. *International Journal of Smart and Nano Materials*, *2(3)*, 194-218, doi: 10.1080/19475411.2011.594105

[6] He, K. & Zhu, W.D. (2011). Damage Detection of Space Frame Structures with L-shaped Beams and Bolted Joints Using Changes in Natural Frequencies. *Proceedings of the 23rd ASME Biennial Conference on Mechanical Vibration and Noise*, Washington, DC, Aug. 28-31, 2011, doi:10.1115/DETC2011-48982

[7] He, K. & Zhu, W.D. (2011). Detecting Loosening of Bolted Connections in a Pipeline Using Changes in Natural Frequencies. *Proceedings of the 23rd ASME Biennial Conference on Mechanical Vibration and Noise*, Washington, DC, Aug. 28-31, 2011.

[8] Lin, R.J. & Cheng, F.P. (2008). Multiple crack Identification of a Free-free Beam with Uniform Material Property Variation and Varied Noised Frequency. *Engineering Structures*, *30*, 909-929.

[9] Ganeriwala, S.N., Yang, J. & Richardson, M. (2011). Using Modal Analysis for Detecting Cracks in Wind Turbine Blades. *Sound and Vibration.*, *45(5)*, 10-13.

[10] Das, P. (2012). Detection of Cracks in Beam Structures Using Modal Analysis. *Applied Mechanics and Materials*, *105-107*, 689-694, doi: 10.4028/www.scientific.net/AMM.105-107.689

[11] Swamidas, A.S., Yang, X. & Seshadri, R. (2004). Identification of cracking in beam structures using Timoshenko and Euler formulations. *J. Eng. Mech., 130(11)*, 1297–1308, doi: 10.1061/(ASCE)0733-9399(2004)130:11(1297)

[12] Caddemi, S. & Calio, I. (2009). Exact closed-form solution for the vibration modes of the Euler-Bernoulli Beam with multiple open cracks. *J. Sound and Vibration*, *327*, 473-489, doi:10.1016/j.jsv.2009.07.008

[13] Rubio, L. (2011). An Efficient Method for Crack Identification in Simply Supported Euler-Bernoulli Beams. *Journal of Vibrations and Acoustics*, *131*, 051001-1 to 051001-6.

[14] Krawczuk, M. & Ostachowicz, W.M. (1995). Modeling and Vibration Analysis of a Cantilever Composite Beam with a Transverse open crack. *J. Sound and Vibration, 183(1)*, 69-89.

[15] Dimarogonas, A.D. (1996). Vibration of Cracked Structures: A State of the Art Review. *Engineering Fracture Mechanics, 55(5)*, 831-857.

[16] Chatterjee, A. (2011). Nonlinear Dynamics and Damage Assessment of a Cantilever Beam with Breathing Edge Crack. *J. Vibration and Acoustics, 133(5)*, 051004-1 to 051004-6.

[17] Liu, J., Zhu, W.D., Charalambides, P.G., *et al.* (2016). Four-beam Model for Vibration Analysis of a Cantilever Beam with an Embedded Horizontal Crack. *Chinese Journal of Mechanical Engineering*, *29(1)*, 163-179. DOI: 10.3901 / CJME.2015.0901.108.

[18] Fang, X. (2013). The Mechanics of an Elastically Deforming Cantilever Beam with an Embedded Sharp Crack Subjected to an End Transverse Load. Ph.D. Dissertation. Department of Mechanical Engineering, The University of Maryland, Baltimore County. December 2013.

[19] Fang, X. & Charalambides, P.G. (2015). The Fracture Mechanics of Cantilever Beams with an Embedded Sharp Crack under End Force Loading. *Engineering Fracture Mechanics*, *149*, 1-17, doi: 10.1016/j.engfracmech.2015.09.039

[20] Pandey, A.K., Biswas, M. & Samman, M.M. (1991). Damage Detection from Changes in Curvature Mode Shapes. *J. Sound and Vibration*, *145(2)*, 321-332.

[21] Ratcliffe, C.P. (2000). A Frequency and Curvature Based Experimental Method for Locating Damage in Structures. *J. Vibration and Acoustics*, *122(3)*, 324-329.

[22] Ratcliffe, C.P. & Crane, R.M. (2005). Structural Irregularity and Damage Evaluation Routine (SIDER) for Testing of the ½-Scale Corvette Hull Section Subjected to UNDEX Testing. *NSWCCD-65-TR-2005/24*.

[23] Crane, R.M., Ratcliffe, C.P., Gould, R. & Forsyth, D.S. (2006). Comparison Of The Structural Irregularity And Damage Evaluation Routine (SIDER) Inspection Method With Ultrasonic And Thermographic Inspections To Locate Impact Damage On An A-320 Vertical Stabilizer. *Proceedings of the 33rd Annual Review of Progress in Quantitative Nondestructive Evaluation*, July 30 – Aug 4, 2006, Portland, OR .

[24] Timoshenko, S.P. (1921). On the correction factor for shear of the differential equation for transverse vibrations of bars of uniform cross-section. Philosophical Magazine, p. 744.

[25] Cowper, G.R. (1966). The Shear Coefficient in Timoshenko's Beam Theory. *ASME*, *J. Appl. Mech.*, *33*, 335-340.

[26] Rice, J.R. (1968). A Path Independent Integral and the Approximate Analysis of Strain Concentration by Notches and Cracks. *J. Appl. Mech.*, *35*, 379-386.

[27] Rice, J.R. (1988). Elastic Fracture Mechanics Concepts for Interfacial Cracks. *J. Appl. Mech.*, *55*, 98-103.

[28] Charalambides, P.G., Lund, J., Evans, A.G. & McMeeking, R.M. (1989). A Test Specimen for Determining the Fracture Resistance of Bimaterial Interfaces. *J. Appl. Mech.*, *56(1)*, 77-82.

[29] Charalambides, P.G. (1991). Steady-State Delamination Cracking in Laminated Ceramic Matrix Composites. *J. Am. Ceram. Soc.*, *74(12)*, 3066-3080.

[30] Hutchinson, J.W. & Suo, Z. (1992). Mixed-mode cracking in layered materials. *Advances in Applied Mechanics*, *29*, 63-191.